Geomechanics for Energy and the Environment 5 (2016) 29–41

Contents lists available at ScienceDirect

Geomechanics for Energy and the Environment

journal homepage: www.elsevier.com/locate/gete

Freeze damage of grouting materials for borehole heat exchanger: Experimental and analytical evaluations

Selçuk Erol [1], Bertrand François *

Université Libre de Bruxelles (ULB), Building, Architecture and Town Planning Dept (BATir), Laboratoire de GéoMécanique, Avenue F.D. Roosevelt, 50 - CPI 194/2, B - 1050 Bruxelles, Belgium

HIGHLIGHTS

- We developed an analytical model to predict freeze damage of borehole heat exchange.
- The model prediction is compared with obtained results on an experimental set-up.
- Crack occurrence predicted by the model agrees well with experimental observation.
- Permeability and porosity of grout have primary role on the freeze-induced failure.

ARTICLE INFO

Article history:
Received 29 September 2015
Received in revised form 17 November 2015
Accepted 16 December 2015
Available online 31 December 2015

Keywords:
Grouting material
Frozen pore water pressure
Thermal stress
Hollow cylinder
Analytical solution
Ground source heat pump

ABSTRACT

The closed-loop ground source heat pump (GSHP) systems can be operated below the freezing point of water with anti-freeze mixture through the installed borehole heat exchangers (BHE) in the ground for the heating purposes of buildings. During the operations, the BHE is exposed by the thermal stresses due to heat loading. In addition if the porous grout material is immerged in water, the freezing-induced ice pressure may damage the grout. In this paper, the freezing impact on BHEs is investigated analytically and experimentally. For the theoretical approach, an analytical solution is developed by using the hollow cylinder model that accounts for both the high density polyethylene (HDPE) pipe and the grout material. Firstly, the frozen pore water pressure is incorporated in the generalized Hooke's law equations in 2D plane stress, and secondly the model is solved for the considered boundary conditions. In order to validate the developed model, the experimental setup is conducted in agreement with the geometry of the considered analytical model and the BHE specimens are prepared with three different grout materials having large difference in the thermal and hydraulic characteristics (i.e. silica-sand based, calcite based and homemade thermally enhanced with graphite). According to the experiments for 50 h of freezing operation, the calcite based grout and the homemade grout, having lower permeability and relatively higher porosity, are fractured. In contrast, the silica-sand based grout having higher permeability did not exhibit any damage. Compared with the theoretical results, the observations from the experiments are consistent. The effective tangential stress induced by the frozen pore water pressure causes the crack development and agrees with the crack patterns. It is concluded that the porosity and the permeability play significant role on the grout failure upon freezing.

1. Introduction

In the context of geological energy production, borehole heat exchangers (BHEs) allow to extract or store

* Corresponding author. Tel.: +32 2 650 27 35; fax: +32 2 650 27 43.
E-mail addresses: selcuk.erol@ulb.ac.be (S. Erol), bertrand.francois@ulb.ac.be (B. François).
[1] Tel.: +32 2 650 27 46.

http://dx.doi.org/10.1016/j.gete.2015.12.002
2352-3808/

heat from the ground. Those operations may modify significantly the temperature of the ground and produce thermo-mechanical disturbance of the system. In particular, for heating purposes, BHEs can be operated below the freezing point of water with the heat carrier fluid, and the anti-freeze mixture circulating through the pipes. This operation at low temperatures not only causes contraction of the backfilling materials, but also freezing of the water inside the pores of the grout with an expansion of growing ice-lenses. These complex hydraulic and thermo-mechanical behaviors may damage the grout. Therefore, in order to avoid an early-damage on the geothermal installation due to the system overload during the peak demands, the grout material used for ground source heat pump (GSHP) systems should be frost-resistant to sustain the heat transfer between the ground and the pipes, and also to prevent aquifers from pollution, most likely, due to the leaking of anti-freeze mixture.

The freezing of pore water is a non-linear heat transfer process which leads the concurrent changes of thermo-hydro-mechanical properties. For a borehole heat exchanger in an infinite ground medium, the ice growth is controlled by the heat source and the permeability of the medium. Based on the mechanism of growing ice formations in the pores, some theoretical models are described in the literature. Among the pioneering investigations about the freezing of porous materials, Powers and Helmuth[1] presented a model of hydraulic pressure inside the pores. On the one hand, their model predicts that the larger pores freeze faster than the small ones causing high hydraulic pressure and cracks in the material. On the other hand, the pores that contain empty air voids slow down the growing ice formations. Litvan[2] provided a theoretical model which demonstrates that the surface forces of pores play a significant role to hinder the freezing process. More recent studies present models to approximate the pressure in the fully water-saturated pores involving the stress and strain states during freezing of porous materials.[3–6] Vlahou and Worster[5] investigated the symmetrically growing ice lens in a spherical cavity within a porous rock as a function of permeability. The high permeability allows water to flow easily to release the pressure. In contrast, low permeability causes a reduction in the ice formation in the cavity, but it increases the pressure by a thin water film acting as the disjoining force to separate the ice and the rock. These forces expand and open new paths enhancing the ice formation by sucking water toward the ice front. Furthermore, Walder and Hallet[7] showed that the rate of the ice growth considerably increases in a temperature range of −4 °C to −15 °C. If the temperature range is more than −4 °C and close to 0 °C, the existing pore ice cannot increase the pressure sufficiently to lead to a significant fracture.

Concerning experimental works about the freezing of porous materials, most of the studies focus on the determination of the resistance of concrete mortar or Portland-cement paste to the freeze-thaw cycles caused by surface temperature conditions.[8–13] In some situations, the durability of the materials can be clearly jeopardized by the mechanical impact of freezing. Borinaga-Treviño et al.[14] summarized all these experimental studies showing the applied methods and the boundary conditions directly applied to the issue of borehole heat exchanger. According to Borinaga-Treviño et al.,[14] except the cement, the mortars containing limestone or silica-sand are not affected by the freeze-thaw cycles. However, in contrast, they also mentioned that, due to the larger thermal expansion coefficient of the HDPE pipe (the thermal expansion coefficient being approximately 10 times higher compared to the mortar), the HDPE pipe creates tangential tension in the mortar and causes a failure in the pipe/grout interface and the crack propagates until the overall failure. This observation clearly underlines that the freeze-thaw damage is not only a function of the freezing resistance of the porous material itself, but also on the boundary conditions and the interactions with the other systems (i.e. pipes, ground).

In order to ensure a frost-proof grout material for a BHE, a standard method for freeze-thaw cycles can be conducted, but the established norms refer only to conventional applications and do not consider the specific case of BHE. Herrmann[15] conducted three different tests to investigate the reliability of grouting materials for freeze-thaw cycles. Two methods are in accordance with the standard test methods DIN 52104-1 and DIN CEN/TS 12390-6, and the third method is more oriented to the practical temperature range with a single-pipe geothermal BHE specimen. According to Herrmann,[15] the standard test method DIN 52104-1 is not suitable for grout material, because the samples are fatally damaged after only one freeze-thaw cycle and unable to perform any measurement test after the experiment. The applied temperatures on the samples are considerably lower than for a GSHP system (i.e. −20 °C). The DIN CEN/TS 12390-6 provided comparatively more reasonable results. The freeze-thaw cycles cause fractures on most of the ready-made grouts and lead to a decrease of 4%–20% on the thermal conductivity while the permeability values are raised by up to one order of magnitude. The third method is to operate a small-scale BHE specimen under dry sand or water-saturated sand conditions, to monitor the temperature distribution in the vicinity of the BHE specimen and to observe visible damage of the specimen after dismantling. According to their results, under low thermally conductive ground, the impact of freeze-thaw cycles is more significant on the BHE specimens due to lower thermal gradient. Recently, Anbergen et al.[16] studied the behavior of BHEs submitted to freeze-thaw cycles, by measuring the permeability of different grouted single-pipe BHE specimens with a parameter setup. According to Anbergen et al.,[16] the grouted specimens containing swelling clay minerals reduce the impact of freeze-thaw cycles on the permeability, because the micro-fractures that occurred due to thermal stresses are likely filled with swelling clay in the grout.

The resistance of grout/mortar materials has already been studied by many authors. Therefore, the objective of the present study is to understand the hydro-thermal and thermo-mechanical behavior of porous grout materials used for GSHP systems to determine how the freezing process causes the degradation on a grouted BHE. This study combines some laboratory experiments with theoretical approaches. The theoretical model used to evaluate the stress in a freezing BHE is derived by an analytical solution considering a hollow cylinder model. For the experimental part, similar to the hollow cylinder approach,

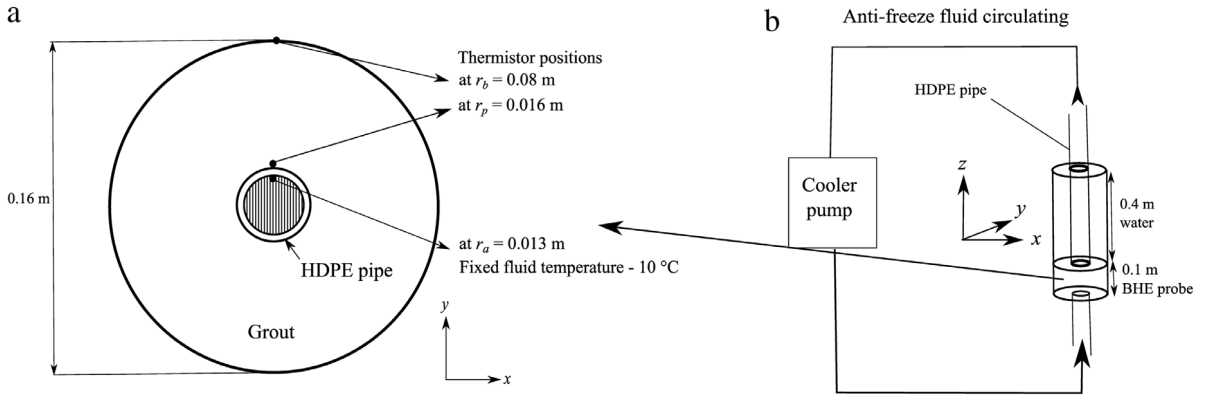

Fig. 1. Illustration of the BHE specimen with thermistor positions.

Table 1
Dimensions and characteristics of BHE specimen.

Parameters		Value
Radius of BHE	r_b	0.08 m
Length of BHE specimen	H_b	0.1 m
Outer radius of the pipe	r_p	0.016 m
Inner radius of the pipe	r_a	0.013 m
Volumetric flow rate inside the pipes (Reynold number 4.7×10^3 at -10 °C)	Q_f	3.66×10^{-4} m^3 s^{-1}
Ambient temperature	T_A	15 °C

the BHE comprises a single HDPE pipe in the middle of the specimen and is surrounded by grout material. The system is operated with anti-freeze mixtures at the temperature of −10 °C during 50 h.

2. Experimental setup

The objective of the experiment is to evaluate the impact of the thermo-hydraulic and mechanical characteristics of the grout material on the freezing-induced damage.

The BHE specimens are prepared in the moisture resistant carton tube with the height of ∼0.5 m. These tubes are mostly used to form the cement in a cylinder shape. The fresh grout material is molded inside the tube approximately 10 cm of height and the rest of the column tube is filled with water (Fig. 1(b)). Afterwards, the fresh specimen is cured for 28 days under water, and the saturation is fulfilled with the gravity. During the operations, the temperature distribution is monitored in the specimens with the thermistor placed at the outer-wall of the HDPE pipe r_p, at the borehole wall r_b and the inner wall of the HDPE pipes r_a in which the anti-freeze mixture circulates (Fig. 1).

The circulating fluid in HDPE pipes is a mixture of 75% water and 25% Ethylene-glycol (purity 93%). This is an optimum percentage of an admixture to avoid increasing excessively the viscosity of the fluid. The specimens are operated for 50 h with the temperature of circulating anti-freeze fluid set to −10 °C. The temperature of the heat carrier fluid is nearly the freezing limit of the admixture. After a thawing period of a few days, the specimens are dismantled and the integrity of the grout is visually checked. The characteristics of BHE specimens are given in Table 1.

Three different grout materials have been considered, and with each kind of grout material two BHE specimens are prepared and operated to obtain comparative results. Two grouts materials are widely used commercial products for BHEs (a thermally enhanced silica-sand based material and a calcite based material having lower thermal conductivity and lower permeability). The third material is a homemade grout containing natural graphite powder.[17] The homemade grout has a high thermal conductivity as the silica-sand based grout and lower permeability as the calcite based grout. The thermo-mechanical and hydraulic properties of grouting materials and geothermal HDPE pipes are given in Table 2.

The intrinsic permeability values given in Table 2 are measured directly in a BHE specimen in which pressure can be applied on the top, and the water flow rate can be measured.

3. Thermo-mechanical model

3.1. Temperature distribution in BHE

The objective of this section is to model the temperature evolutions obtained experimentally in the specimen with an existing theoretical model. Classical GSHP systems are operated by fixing the heat extraction rate while the heat carrier fluid temperature and the borehole wall temperature evaluated in time will depend on the assigned heat exchange rate. In the present study, since the aim is to estimate the failure of the grout material under freeze-thaw cycles of a BHE, the temperature of the heat carrier fluid is fixed. Certainly, the heat carrier fluid temperature will cause the phase change of the pore water which may have an impact on the thermal properties of the BHE constituents. However, to keep the thermal transfer equations relatively straightforward, this effect of phase

Table 2
Parameters of laboratory setup components.

	Parameters	HDPE pipe	Silica-sand based grout	Calcite based grout	Homemade grout
Linear thermal expansion coef.	α (K^{-1}) $\times 10^{-5}$	12[a]	1.4[c]	1.3[c]	1.4[c]
Young modulus	E (Pa) $\times 10^{9}$	1.45[a]	6.5[d]	5.5[d]	5[d]
Permeability coefficient	κ (m^2)[e]	–	1.8×10^{-14}	7.1×10^{-17}	9×10^{-16}
Porosity	n (–)[f]	–	0.12	0.31	0.18
Poisson ratio	υ (–)	0.45[a]	0.21[g]	0.21[g]	0.21[g]
Volumetric heat capacity	ρc (J kg^{-1} m^{-3}) $\times 10^{6}$	2[b]	2.7[d]	2.5[d]	2.55[d]
Thermal conductivity	λ (W m^{-1} K^{-1})	0.42[b]	2.3[d]	0.9[d]	2.3[d]

[a] Ref. [18].
[b] Ref. [19].
[c] Ref. [20] depending on the mineral.
[d] Ref. [17].
[e] Measured values of BHE specimen including HDPE pipe.
[f] Measured values.
[g] Ref. [21].

change of water is disregarded. This is justified because the grout material is relatively dense such that the water phase occupies a limited volume of the mixture leading to a reduced effect of the latent heat. In order to evaluate the temperature change in a BHE, cylinder or line heat source models can be used.[22,23] The assumption of the cylinder source model takes into account the overall temperature response including the pipe and the grout together, which we need to calculate separately. Therefore, the traditional heat line source model is considered to deduce the temperature change at the pipe wall and at the borehole wall in the BHE and to compare the analytical solution with experimental results.

In order to evaluate the temperature changes at the outer wall of the HDPE pipe and at the borehole wall, the temperature gradient should be determined with respect to the thermal resistance of the specimen constituents and the heat exchange rate. The line source analytical model described for the heat transfer between borehole and the infinite region can be used to calculate the heat exchange rate as a time dependent solution[24]:

$$\psi(t) = \frac{\Delta T_a}{\frac{1}{4\pi\lambda_s} E_1\left(\frac{r_b^2}{4tD_s}\right) + Rs_b} \tag{1}$$

in which ψ is the heat exchange rate, λ_s is the bulk thermal conductivity of the ground, r_b is the radius of specimen, D_s is the thermal diffusivity of ground, ΔT_a is the temperature change at r_a (in the pipe, imposed in our case) and $E_1(r_b^2/4tD_s)$ is the exponential integral function. Rs_b is the borehole thermal resistance[25]:

$$Rs_b = \underbrace{Rs_{conv} + Rs_{cond}}_{Rs_p} + Rs_g. \tag{2}$$

The total borehole thermal resistance includes pipe resistance Rs_p (decomposed into convection and conduction resistance Rs_{conv} and Rs_{cond}, respectively) and the grout thermal resistance Rs_g. The two pipe resistances are given as follows:

$$Rs_{conv} = \frac{1}{2\pi r_a \vartheta} \tag{3}$$

$$\vartheta = \frac{\mathrm{Nu}\lambda_f}{2r_a} \tag{4}$$

$$Rs_{cond} = \frac{\ln(r_p/r_a)}{2\pi\lambda_p} \tag{5}$$

in which r_a and r_p are the inner and outer radius of pipes, respectively. ϑ is the heat transfer coefficient estimated with Nusselt number (Nu), inner radius of the pipe r_a and thermal conductivity of the anti-freeze fluid λ_f.

The grout has a hollow cylinder shape, and the thermal resistance can be obtained as[26]:

$$Rs_g = \frac{\ln r_b/r_p}{2\pi\lambda_g} \tag{6}$$

in which λ_g is the thermal conductivity of grout material.

The temperature difference between the heat source and the borehole wall is proportional to the heat exchange rate and the thermal resistances of HDPE pipe and grout. This can be decomposed into two temperature differences: one for the pipe and another for the grout. Consequently, the temperature differences at the outer wall of the HDPE pipes ΔT_p and of the grout ΔT_b are calculated as follows[27]:

$$\Delta T_p(t) = \Delta T_a - \psi(t) Rs_p \tag{7}$$

$$\Delta T_b(t) = \Delta T_a - \psi(t) Rs_b. \tag{8}$$

3.2. Ice pressure in porous grout material

The phase change of water is traditionally described as the Stefan's freezing problem.[28] In fact, the ice growth in a porous material is governed by not only the heat flux, but also the water flow mechanism in pores that drives the solidification front of growing ice lens. When the thermodynamic and the flow conditions are in equilibrium for the pore pressure of water, these two mechanisms can be combined to evaluate the disjoining pressure between ice and particle.

There are several approaches to estimate the disjoining pore water pressure by combining the thermodynamic equilibrium at the solid/water interface as the Clausius–Clapeyron equation with the governing equation of the Stefan's freezing problem.[3,5,6,29]

Based on the concept of spherical pores and spherical ice lenses, as developed by Vlahou and Worster,[5] the freezing process of pore water is illustrated in Fig. 2. In the early stage of the freezing, the growing ice thrusts the

water through the pore throats. If the water inside the pore cannot dissipate fast enough due to smaller throats, liquid pressure increases. At the later stage, when the ice lens reaches the pore wall, the ice pushes the grout matrix and may cause a possible failure of the material.

In order to calculate the total ice pressure depending on the freezing conditions, the mass and volume changes of water in pores should be taken into account. Penttala[3] derived the freezing-induced disjoining pressure in a porous material $p_T(T)$, taking into account the change in the specific volume accounting for a constant mass of water in the pores. This assumption is valid only upon undrained conditions, characteristic of very low permeability material for which the water present in the pore cannot be expelled out during the freezing process. The resulting pressure is approx. -11 MPa K^{-1} which constitutes clearly an overestimation of the ice pressure. Therefore, we estimate the disjoining pore pressure by taking into account the change in water mass based on the approach of Vlahou and Worster.[5] This implies that water mass exchange can occur through the pore throats, according to the concept sketched in Fig. 2. Therefore, we considered the Clausius–Clapeyron equation that gives the pressure at the ice–water interface for local thermodynamic equilibrium[6]:

$$p_T = p_l - p_i = \left(p_l - \left(\frac{1}{\rho_i} - \frac{1}{\rho_l} \right)^{-1} L \frac{\Delta T}{T_0} \right). \tag{9}$$

This pressure acts as a disjoining pressure between liquid and ice. ΔT is the difference of temperature between the melting temperature of liquid T_0 ($T_0 = 0$ °C in our case) and the temperature at the solidification interface T_{interf}. The second term is the ice pressure p_i. p_l is the liquid pressure in pore, ρ_i and ρ_l is the bulk density of ice and liquid water, respectively. L is the latent heat of phase change.

The liquid pressure in a pore can be obtained as a function of the rate of ice growing, combined with the rate of water flow out of the pore. The rate of water mass change is given by:

$$\begin{aligned} \frac{\Delta m}{\Delta t} &= \frac{\Delta (m_l + m_i)}{\Delta t} = \frac{\Delta (V_l \rho_l + V_i \rho_i)}{\Delta t} \\ &= \frac{\partial V_i}{\partial t} (\rho_i - \rho_l) = \frac{\partial V_i}{\partial a} \frac{\partial a}{\partial t} (\rho_i - \rho_l) \\ &= 4\pi a^2 \frac{\partial a}{\partial t} (\rho_i - \rho_l) \end{aligned} \tag{10}$$

where V_i is the volume of the ice sphere of radius a. This equation is obtained considering that, during the ice formation, the ice occupies the volume previously occupied by water, $\Delta V_l = -\Delta V_i$. This equality assumes that the radius of the pore remains constant during the ice formation. This assumption is justified by the low magnitude of the liquid pressure in regard with the relatively high stiffness of the grout material combined with the small radius of the pore. Vlahou and Worster[5] proposed an extension of their method to consider the cavity expansion. In the present case, we have checked that this additional effect can be disregarded.

The liquid water mass flow q_m out of the pore sphere can be expressed with respect to the pressure gradient

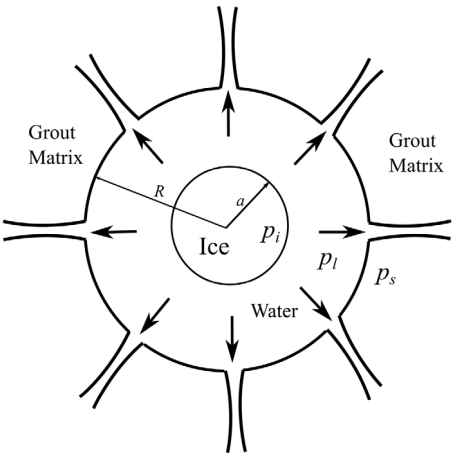

Fig. 2. Illustration of pore water freezing in a spherical cavity. *Source:* Adapted from Ref. [5].

according to Darcy's law:

$$q_m = vA\rho_l = -\overbrace{\frac{\kappa}{\mu_0} \frac{\partial p_l}{\partial r_{pore}}}^{v} \overbrace{4\pi r_{pore}^2}^{A} \rho_l \tag{11}$$

in which κ is the intrinsic permeability, μ_0 is the dynamic viscosity of water at 0 °C and r_{pore} is the radial coordinates in the spherical pore. v and A are the velocity of liquid water and the section through which liquid water flows, respectively.

Under the mass balance of the liquid water, the mass flow q_m out of the pore sphere (Eq. (11)) must be equal to the absolute value of the rate of mass change in the pore (Eq. (10)), leading to:

$$\underbrace{4\pi a^2 \frac{\partial a}{\partial t} (\rho_l - \rho_i)}_{|\Delta m/\Delta t|} = \underbrace{-\frac{\kappa}{\mu_0} \frac{\partial p_l}{\partial r_{pore}} 4\pi r_{pore}^2 \rho_l}_{q_m}. \tag{12}$$

This equality is valid under the assumption that the liquid and solid water are uncompressible, ρ_l and ρ_i being assumed not affected by temperature and pressure. The water pressure inside the pore, function of the radial coordinate inside the pore r_{pore}, can be found by integration of Eq. (12):

$$p_l(r_{pore}, t) = \frac{\partial a}{\partial t} \frac{a^2 \chi \mu_0}{\kappa r_{pore}} \tag{13}$$

where χ the dimensionless constant representing the rate of density $\chi = (\rho_l - \rho_i)/\rho_l$. The liquid pressure that we are interested in (i.e. affecting the mechanical behavior of the solid matrix of grout) is the pressure at the pore boundary, when $r_{pore} = R$:

$$p_l = \frac{\partial a}{\partial t} \frac{a^2 \chi \mu_0}{\kappa R}. \tag{14}$$

Eq. (12) demonstrates that the rise of the liquid pressure results from the water solidification that acts as a source term that pushes the liquid water out of the pore. Consequently, the magnitude of liquid water pressure

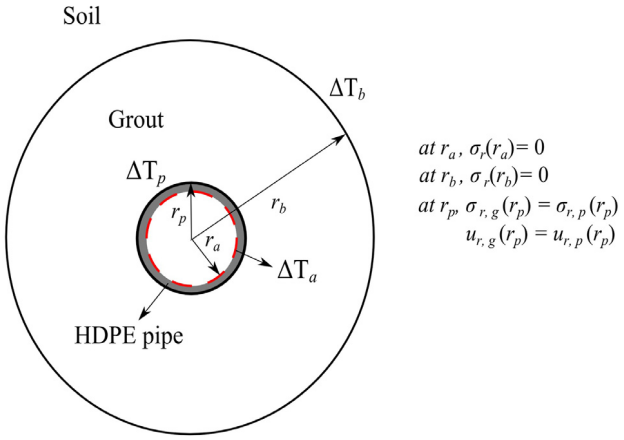

Fig. 3. Illustration of the two combined hollow cylinder problems in HDPE pipe and grout.

depends on the rate of ice growing and the speed at which water can be expelled out of the pore. The rate of growing ice radius $\partial a/\partial t$ can be determined by combining, the Clausius–Clapeyron equation (9) with the liquid pressure equation (14). Setting it into the heat balance equation described as the equation of the Stefan's freezing problem, we obtain the following differential equation (15). The detailed solution can be found in Appendix A.

$$\underbrace{\frac{\partial a}{\partial t}a^2}_{1st} + \underbrace{\frac{\partial a}{\partial t}aR\beta}_{2nd} = \frac{\lambda_l\left(T_0 - T_{interf}\right)}{\rho_i L}R\beta \tag{15}$$

in which T_{interf} is the temperature at the solidification interface between ice and water. β is a dimensionless parameter given as:

$$\beta = \frac{\kappa\rho_w^2\rho_i^2L^2}{\lambda_w\mu_0\Delta\rho^2T_0} \tag{16}$$

where $\Delta\rho = \rho_l - \rho_i$. The ordinary differential equation given in Eq. (15) is an initial value problem of a_0. The pressure-melting effect is represented as the first term on the left hand side of Eq. (15), and the second term is the latent heat flow away from the solidified ice front. According to Vlahou and Worster,[5] if $\beta < 1$ (for very low permeability value of media, $\sim 1 \times 10^{-20}$ m^2), the first term of the left-hand side of Eq. (15) can play a significant role. On the contrary, in our case, the intrinsic permeability value of a typical grout material varies in a range of 1×10^{-14}–1×10^{-18} m^2. Consequently, the first term vanishes due to the relatively large magnitude of β in the second term. Therefore, Eq. (15) can be simplified to obtain the rate of ice sphere growing, as:

$$\frac{\partial a}{\partial t} = \frac{\lambda_i\left(T_0 - T_{interf}\right)}{a\rho_i L}. \tag{17}$$

The combination of Eqs. (14) and (17) leads to the expression of the liquid pressure p_l at the pore wall:

$$\begin{cases} p_l = 0 \quad \text{for } T_{interf} > 273.15 \text{ K} \\ p_l = \dfrac{\lambda_i\left(T_0 - T_{interf}\right)}{\rho_i L}\dfrac{a\chi\mu_0}{R\kappa} \\ \quad \text{for } T_{interf} < 273.15 \text{ K}. \end{cases} \tag{18}$$

For a freezing period of several hours and for the encountered permeability of grouts, the rate of ice sphere growing, governed by Eq. (17) is such that the ice fully fills the pore sphere rapidly. So, at the time $t_{\max}$ (a few seconds for $T_0 - T_{interf} = 5$ °C and $R \approx 10^{-4}$ m), $a = R$, and the liquid pressure becomes independent of the pore size. It is the assumption taken in the results below.

3.3. Analytical model for thermal stress

The problem is addressed as two coupled co-centric hollow cylinders lying on each other.[30] The first one corresponds to the HDPE pipe while the second one is the grout (Fig. 3).

The boundary conditions of the two combined problem are as follow:

- The internal boundary condition of the HDPE pipe for $r = r_a$, and the outer boundary of the grout for $r = r_b$ are free of stress.
- At radius $r = r_p$, the radial stress and radial displacement of the pipe and of the grout are equal. This joined boundary condition (translating the mechanical equilibrium between the grout and the pipe) makes that the two thermo-mechanical problems are coupled.
- Temperature at the inner radius r_a is fixed to a certain value (i.e. −10 °C). The temperature changes at the outer radius of the pipe r_p and at the outer radius of the grout r_b, are evaluated according to Eqs. (1), (7) and (8).

This section demonstrates the main thermo-mechanical equations applied to the hollow cylinder geometry upon plane stress conditions.[31,32] The momentum equilibrium equation in cylindrical coordinates for axisymmetric plane stress problem is:

$$\frac{\partial\sigma_r}{\partial r} + \frac{1}{r}(\sigma_r - \sigma_\theta) = 0 \tag{19}$$

in which σ_r and σ_θ, are the radial and circumferential total stresses, respectively. r is the radial distance. The strain tensor components can be expressed as[31]:

$$\varepsilon_r = \frac{\partial u_r}{\partial r}, \qquad \varepsilon_\theta = \frac{u_r}{r} \tag{20}$$

where u_r is the radial displacement. ε_r and ε_θ are the radial and tangential strains, respectively.

In poroelastic theory,[29,33,34] the deformations and the strengths are governed by the Biot's effective stress obtained from the total stress and pore water pressures as follow:

$$\sigma_{eff} = \sigma_T - p_l b S_l - p_i b S_i \tag{21}$$

where σ_T is the total stress, σ_{eff} is the Biot's effective stress, p_i and p_l are the ice and liquid pressure while S_l and S_i are the saturation ratio of liquid water and ice, respectively:

$$S_i = \frac{V_i}{V_{pore}} = \left(\frac{a}{R}\right)^3; \qquad S_l = \frac{V_l}{V_{pore}} = 1 - S_i. \tag{22}$$

Let us note that for a freezing period of several hours, the pore sphere is rapidly fully filled with ice, leading to a saturation ratio of ice equal to unity while the saturation ratio of water is null. b is the Biot's coefficient which is related to the bulk modulus of drained porous medium (K_0) and the bulk modulus of solid grain (K_s):

$$b = 1 - \frac{K_0}{K_s}. \tag{23}$$

The bulk modulus of the solid grain can be correlated to the total porosity and the bulk modulus of the drained medium[35,36]:

$$K_s = \frac{K_0}{(1 - n^m)} \tag{24}$$

in which n is the total porosity and m is a material parameter, taken equal to 3 for hydrated cement pastes.

In order to determine the stress–strain relationship including the pore pressures upon non-isothermal conditions in cylindrical coordinates for linear thermo-elastic and isotropic material, the Biot's poroelastic approach[35] and the generalized Hooke's law in 2D plane-stress equations can be combined as[34]:

$$\sigma_{r,T} = \frac{E}{1-\nu^2}(\varepsilon_r + \nu\varepsilon_\theta - \delta T\alpha(1+\nu)) + p_l b S_l + p_i b s_i \tag{25}$$

$$\sigma_{\theta,T} = \frac{E}{1-\nu^2}(\varepsilon_\theta + \nu\varepsilon_r - \delta T\alpha(1+\nu)) + p_l b S_l + p_i b s_i \tag{26}$$

where E is Young's modulus, υ is Poisson's ratio, α is the coefficient of linear thermal expansion. The term, $\delta T\alpha(1+\nu)$, incorporates the thermal effect of a temperature change on the stress state. The sign convention considers tensile stress as positive, compression stress and pore pressures as negative.

If the equations of the generalized stress components (Eqs. (25) and (26)) are expressed with the particular solutions of strain given in Eq. (20) and are set into the momentum equilibrium equation (Eq. (19)), the obtained partial differential equation must be solved to evaluate the stresses occurred in the materials. The solution of the integration is provided in Appendix B. The integration of the equations gives the stresses in the pipe as:

$$\sigma_{p,r}(r_{a-p}) = E_p\left(\frac{A_p}{1-\nu_p} - \frac{\alpha_{Lp}S_p(r_{a-p})}{r_{a-p}^2} - \frac{B_p}{(1+\nu_p)r_{a-p}^2}\right) \tag{27}$$

$$\sigma_{p,\theta}(r_{a-p}) = E_p\left(\frac{A_p}{1-\nu_p} + \frac{\alpha_{Lp}S_p(r_{a-p})}{r_{a-p}^2} + \frac{B_p}{(1+\nu_p)r_{a-p}^2} - \delta T_p(r_{a-p})\alpha_{Lp}\right) \tag{28}$$

in which r_{a-p} represents the radial coordinate between r_a and r_p. Similarly, the effective stress components in the grout are:

$$\sigma_{g,r-eff}(r_{p-b}) = E_g\left(\frac{A_g}{1-\nu_g} - \frac{\alpha_{Lg}S_g(r_{p-b})}{r_{p-b}^2} - \frac{B_g}{(1+\nu_g)r_{p-b}^2}\right) + (p_l S_l + p_i S_i)(1-\nu_g)b \tag{29}$$

$$\sigma_{g,\theta-eff}(r_{p-b}) = E_g\left(\frac{A_g}{1-\nu_g} + \frac{\alpha_{Lg}S_g(r_{p-b})}{r_{p-b}^2} + \frac{B_g}{(1+\nu_g)r_{p-b}^2} - \delta T_g(r_{p-b})\alpha_{Lg}\right) + \nu_g(p_l S_l + p_i S_i)b \tag{30}$$

in which r_{p-b} represents the radial coordinate between r_p and r_b. $S(r)$ is the integral of the Laplacian temperature δT (see Appendix C). A and B are the integral constants which are evaluated as a function of the boundary conditions, in Appendix D. Four constants are evaluated as: A_g and B_g for the grout problem and A_p and B_p for the pipe problem.

In a hollow cylinder submitted to an axisymmetric temperature field, the temperature distribution along the radius can be expressed as a function of the temperature at the two boundaries, as follows[32]:

$$\delta T(r,t) = \Delta T_{in}(t)\frac{\ln\left(\frac{r_{out}}{r}\right)}{\ln\left(\frac{r_{out}}{r_{in}}\right)} + \Delta T_{out}(t)\frac{\ln\left(\frac{r_{out}}{r}\right)}{\ln\left(\frac{r_{in}}{r_{out}}\right)} \tag{31}$$

where r is the radial coordinate, ΔT_{in} and ΔT_{out} are the temperature variation at the boundaries r_{in} and r_{out} which can be obtained as time dependent for continuous heat loading as described in Section 3.1. Typically, Eq. (31) assumes steady-state condition. However, in our case, the time-dependent effect is taken into account through the temperature evolution at the boundaries of the problem ($\Delta T_{in}(t)$ and $\Delta T_{out}(t)$), the evolution of the temperature profile being treated as a succession of steady-state conditions. In fact, the achievement of this approach is valid due to short distance from heat source to the considered borehole wall where the heat transfer reaches to equilibrium within a short time.

Assuming the temperature profile defined by Eq. (31), the integral of the Laplace temperature for pipe $S_p(r)$ and for the grout $S_g(r)$ can be resolved analytically (see Appendix C).

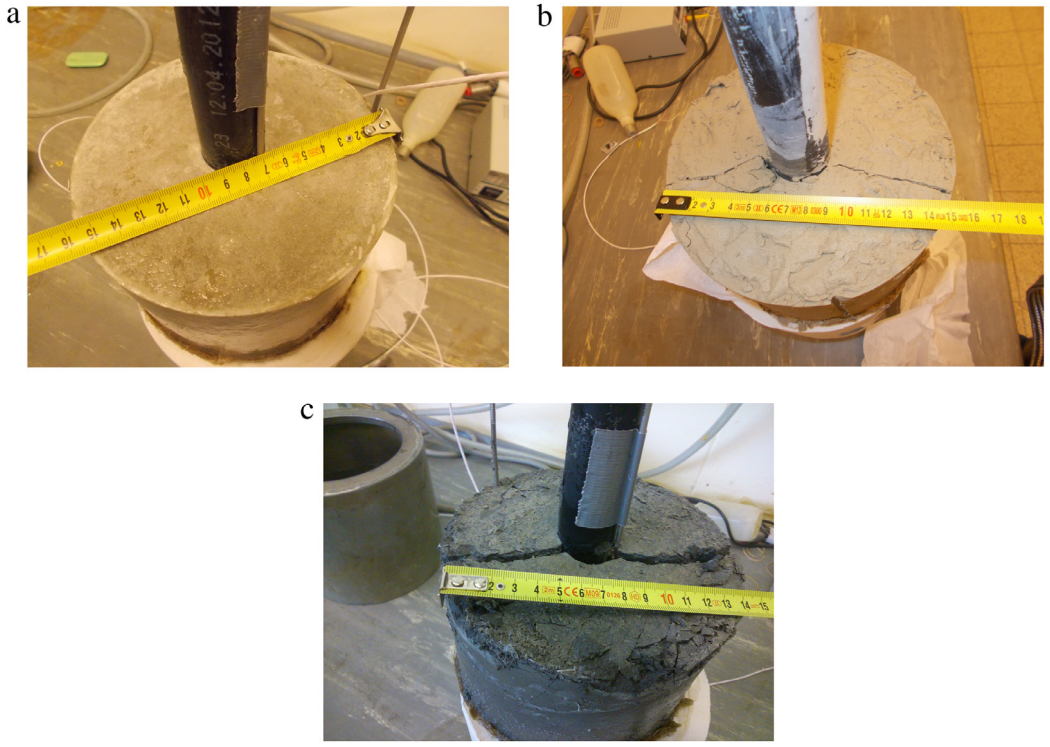

Fig. 4. View of the BHE specimen after dismantling of the experiment: (a) Silica-sand based grout; (b) Calcite based grout; (c) Homemade grout.

4. Results

From an experimental point of view, the BHE specimens, prepared with three different grout materials, are operated for 50 h with the anti-freeze mixture at −10 °C. After a thawing period of a few days, the specimens are dismantled and the integrity of the grout is checked. The occurrence of crack in the specimen is analyzed in relation with stress components obtained theoretically and the strength limits of grout materials, given in Table 3. The grout materials are assumed fully saturated. The visual observations of the specimens after dismantling shown in Fig. 4 demonstrate that the freezing-induced stress causes a crack according to a plane perpendicular to the section of the specimen and directed in the radial direction in the calcite based grout and similarly in the homemade grout. This is characteristic of a failure induced by excessive tangential stress. However the BHE specimen prepared with silica-sand based grout shows no damage. It is important to mention that, for each kind of grout material, two BHE specimens have been tested in the same conditions and the results are identical. Also, it is to mention that we focused our observations on the occurrence of macro-cracks that are continuous and cross the entire specimens. The moment at which those cracks were initiated is unknown (because the observations were done only after dismantling) but the analytical model may provide such information.

In terms of temperature evolutions, Figs. 5–7 demonstrate that the line heat-source model provides satisfactory results. In order to consider the insulation of the BHE specimen in the calculation, the surrounding medium is assumed having poor thermal properties ($\lambda_s = 0.4\,\mathrm{W\,m^{-1}\,K^{-1}}, D_s = 2.5\times10^{-7}\,\mathrm{m^2\,s^{-1}}$). Silica-sand based grout and homemade grout induce similar low temperature gradient in the BHE specimens (Figs. 5 and 6) due to their high and identical thermal conductivity. The calcite based grout has larger thermal gradient due to its lower thermal conductivity compared to other silica-sand based grout and homemade grout. The effect of the latent heat during phase change of pore water (neglected in the analytical prediction) does not seem to be significant, because the materials are considerably denser and the amount of consisting water is small.

Table 3
The strength of grout materials obtained from Brazilian tensile tests and uniaxial compression tests.[17]

Grout material	Silica-sand based	Calcite based	Homemade
σ_c (MPa)	−10/0.388[a]	−9.5/0.141[a]	−7.95/0.212[a]
σ_t (MPa)	1.26/0.0357[a]	1.06/0.0306[a]	1/0.323[a]

[a] Standard deviation. Data given in the table is provided from laboratory measurements, and each grout specimen is performed with 3 samples, and the mean value is taken out of 3 samples.

According to the analytical model, the stresses in the pipe (Fig. 8) show similar magnitude in the three specimens due to similar temperature gradient inside the pipe. It can be seen that there is considerably a large difference of the tangential stress occurred in the pipe and in the grout material due to the thermal expansion coefficient of the pipe that is 10 times larger than the grout.

Considering the total stress results in the grout, the radial stress shows tensile behavior and becomes null

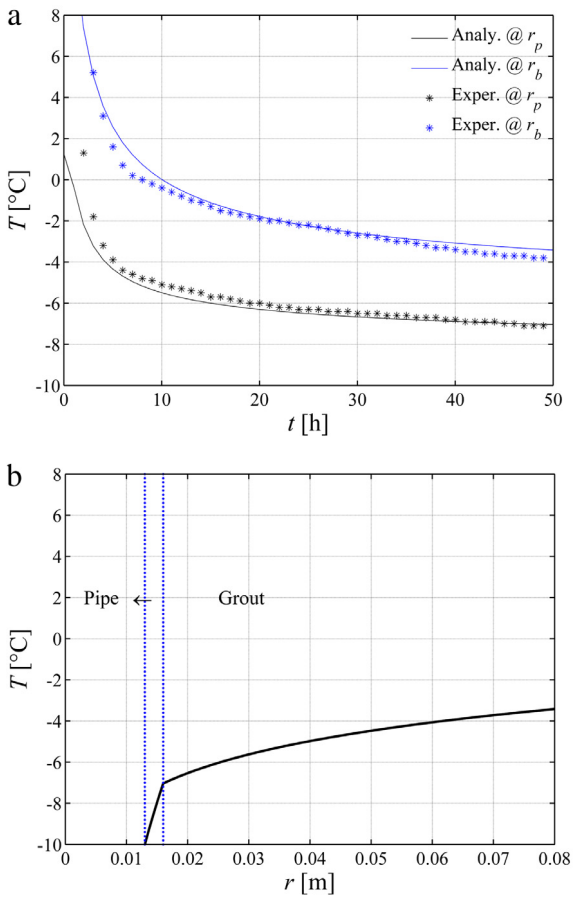

Fig. 5. The temperature evolutions in the Silica-sand based grout: (a) over time comparison between experimental measurement and theoretically calculated results (Eqs. (7) and (8)); (b) over radial distance of the BHEs at 50th h of the operation obtained from analytical solution with Eq. (31).

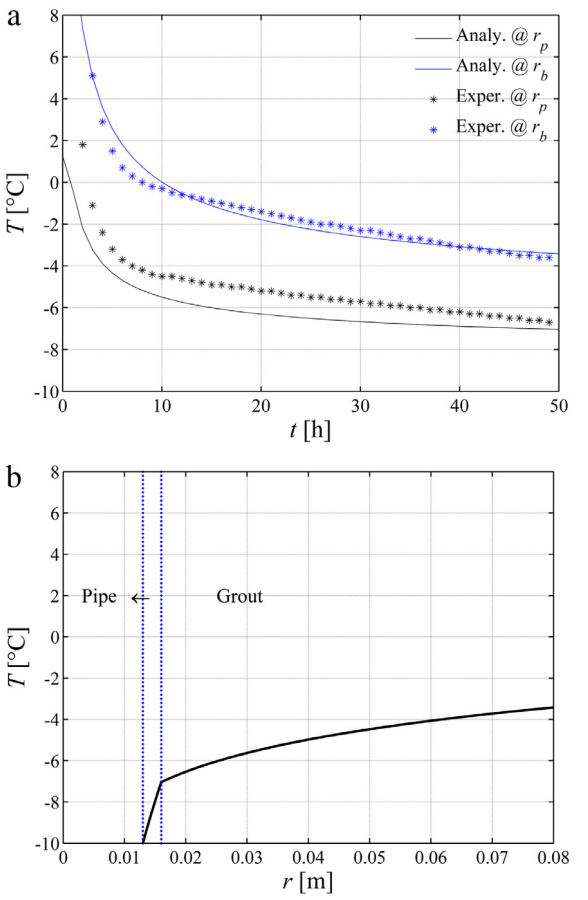

Fig. 6. The temperature evolutions in the homemade grout: (a) over time comparison between experimental measurement and theoretically calculated results (Eqs. (7) and (8)); (b) over radial distance of the BHEs at 50th h of the operation obtained from analytical solution with Eq. (31).

close to the borehole wall, as where the tangential stress mostly shows compressive behavior. The effective stress results demonstrate that the ice pressure shifts both stress components toward tensile behavior. The effective radial stresses of the three grout materials exceeds far from the strength limit of that materials. The effective tangential stress occurred in the silica-sand based grout remains slightly below its strength limit (Fig. 8(a)), as where both in the calcite based grout and in the homemade grout the tangential stress partially exceeds to its limit (Fig. 8(b) and (c)). Regarding to the experimental result shown in Fig. 4(b) and (c), the radial direction of the crack indicates that the failure occurred because the tangential stress exceeds the tensile strength. This is clearly consistent with the analytical model that shows, for calcite based and homemade grouts, effective tangential stresses strongly larger than their tensile strength. The analytical solution is valid only considering an elastic response of the grout. Consequently, once the crack occurs, the model is no more able to represent the stress state in the grout. The occurrence of this radial macro-crack releases the circumferential stress which, in turn, reduces the possible occurrence of additional radial tensile cracks.

It can be mention that the experiments do not exhibit any circumferential macro-cracking (i.e. perpendicular to the radial direction) that would be induced by excessive radial tensile stresses while the analytical solution predicts large radial tensile stress. This is likely because the tensile stress was partially released due to a slight detachment between pipe and the grout, but not visible when the setup was dismantled. In addition, the tangential stress shown in Fig. 8(a) remaining slightly below the tensile strength limit expresses why we do not observe any failure on the silica-sand based grout material.

5. Conclusion

The thermal stress due to heat load of the GSHP systems may impact on the backfilling materials of a BHE, and if the system is operated below the freezing of the pore water, the induced stress including the frozen pore water pressure can cause possible failures in the porous grout material.

In order to study the impact of freezing on a BHE, we developed an experimental setup of small-scale BHE specimens with three different grout materials. In addition,

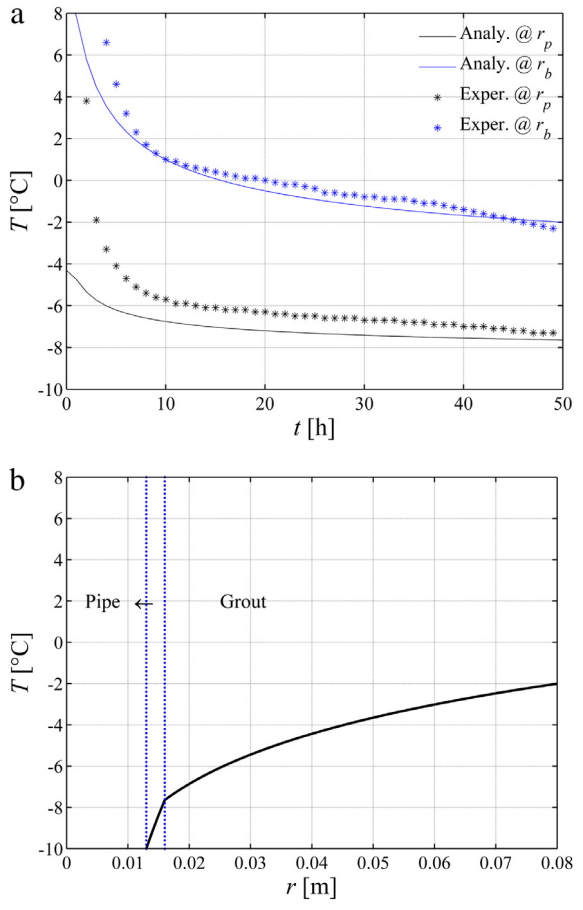

Fig. 7. The temperature evolutions in the calcite based grout: (a) over time comparison between experimental measurement and theoretically calculated results (Eqs. (7) and (8)); (b) over radial distance of the BHEs at 50th h of the operation obtained from the analytical solution with Eq. (31).

we developed a theoretical approach by using a hollow cylinder model to predict the thermally induced stresses both in the HDPE pipe and the porous grout material taking into account the frozen pore water pressure. The ice-pressure in the porous network is deduced based on the assumption that the pores are spherical. On that basis, Gibbs free energy equation, Clausius–Clapeyron's relation, Stefan's freezing problem and Darcy's flow equation are combined to deduce the time and space evolution of ice-pressure. Despite this analytical model is based on a series of simplifications, it shows good agreement with the experimental observations in terms of crack occurrence. So, this study brings, for the first time, an analytical estimation of the freezing impact on the borehole heat exchanger, as a function of the water permeability, thermal conductivity and tensile strength of the grouting material. This analysis is limited to a single pipe geometry in order to fit with the hollow cylinder model used in the analytical framework. To consider more complex geometry, the frozen pore pressure model and its coupling with the mechanical stress should be implemented in a finite element code to solve the problem numerically.

The experimental observations are mainly used to justify the developed analytical model. According to the experimental results, the BHE specimens having lower permeability (i.e. calcite based grout and homemade grout) had a major crack perpendicular to the plane after 50 h of operation, but the silica-sand based grout having considerably larger permeability and lower porosity does not exhibit any damage. The analytical solution demonstrates that, for calcite based and homemade grout the ice pressure causes larger effective tangential stress exceeding the tensile strength limit of the material. This is consistent with the crack patterns observed in the experiment. On the other hand, the calculated effective stress results of silica-sand grout remain below the strength limit that is also in agreement with experiment observations.

It can be concluded that the ice pressure development is controlled by the competition between the rate of ice formation leading to increase pressure, and the rate of water flow inducing pressure dissipation. In case of high permeability, the solidified ice thrusts the water in between the ice and the particle through the larger pore throats such as the water can flow easily and reduce the ice pressure. In contrast, if the material has low permeability the water may not escape fast enough from the ice front due to smaller pore throats and causes larger pressure in pores. Considering the thermal gradient and the permeability of the grout materials, the worst combination may be to have higher thermal conductivity and lower permeability leading faster ice solidification but lower water propagation. The pore volume fraction has also a significant impact on the pressure. By lowering the porosity, the Biot's coefficient is reduced and the proportion of ice pressure transmitted to the solid skeleton is significantly reduced. As a consequence, the durability with respect to freezing can be increased.

According to the present study, if the water/cement ratio is decreased, the porosity can be lowered which may endure the durability of the material. In addition, the grout material having considerably lower permeability and being thermally more conductive may lead to possible crack development. Preferably, the grout material has an equivalent thermal conductivity as the surrounding ground and not extremely low permeability (e.g. $<1 \times 10^{-16}$ m^2) to avoid having larger thermal stress and to reduce the impact of freezing pressure for backfilling materials of BHEs.

Acknowledgment

The financial support from Walloon Region in Belgium is profoundly acknowledged (Grant: 1117492—GeoTherWal–Programme mobilisateur ERable (E24+)).

Appendix A

Hereby we evaluate the differential equation that describes the growing ice radius in a cavity accounting for the pressure-melting effect and the flow of the latent heat away from the ice solidification. The main development is carried out according to the theory of Vlahou and Worster.[5]

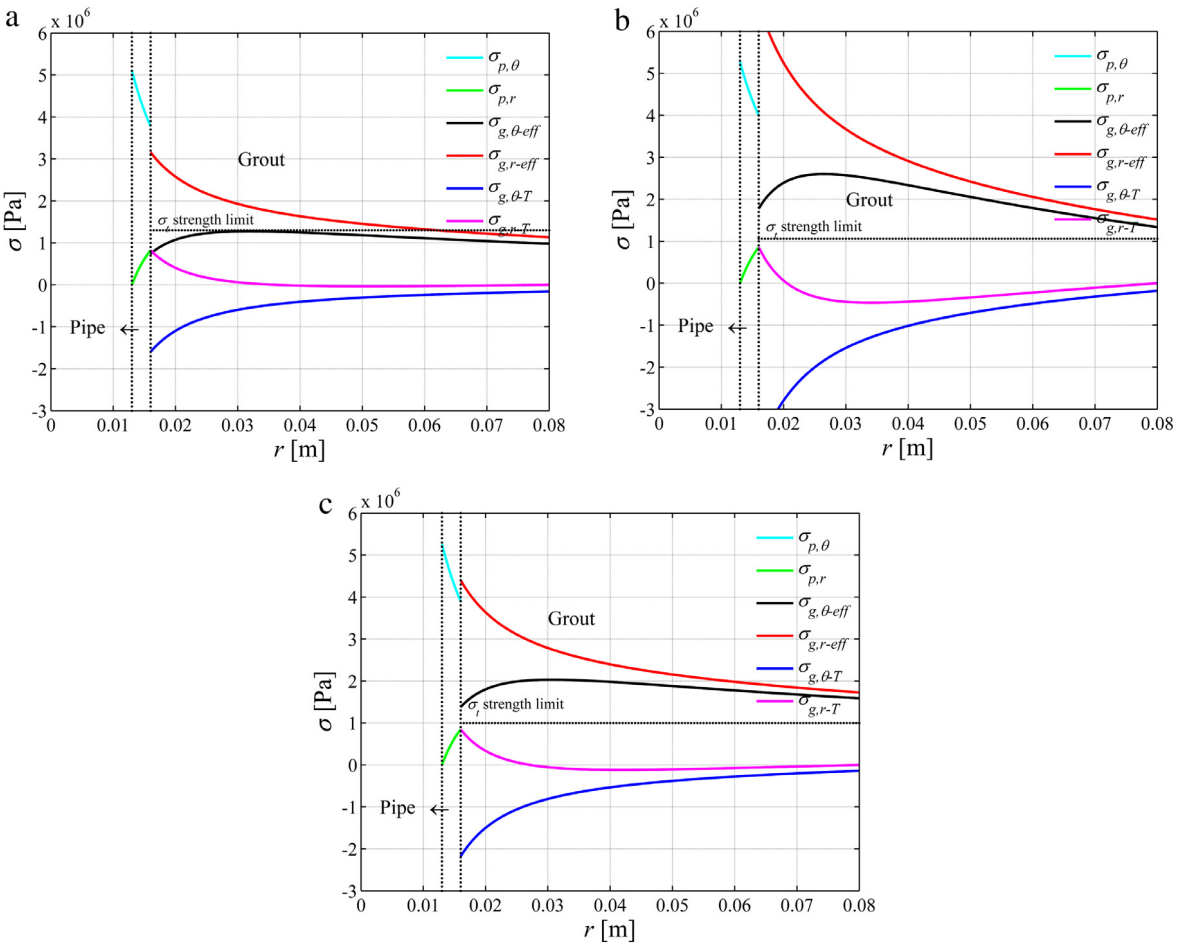

Fig. 8. Total and effective stress components over radial distance of the BHE at 50th h of the operation: (a) Silica-sand based grout; (b) Calcite based grout; (c) Homemade grout.

Firstly, by assuming $p_T = 0$ in the Clausius–Clapeyron equation (Eq. (9)) and combined with the liquid pressure equation (Eq. (14)), Eq. (9) provides the temperature at the solidification interface T_{interf} as:

$$T_{interf} = T_0 \left[1 - \frac{\partial a}{\partial t} \frac{a^2 \chi \mu_0}{\kappa RL} \frac{\Delta \rho}{\rho_i \rho_l} \right] \tag{A.1}$$

where $\Delta\rho = \rho_l - \rho_i$. Here the assumption $p_T = 0$ describes that the disjoining pressure between the ice and the water can be disregarded at the moment when the water starts solidifying and until the ice radius reaches to the pore radius.

When the water freezes, the latent heat due to phase change must be transferred away to continue the freezing process. This phenomenon is called the Stefan's freezing problem and describes the energy conservation at the interface as:

$$\underbrace{\lambda_i \frac{\partial T_i}{\partial r_{pore}}\bigg|_{r_{pore}=a(t)}}_{q_i} - \underbrace{\lambda_l \frac{\partial T_l}{\partial r_{pore}}\bigg|_{r_{pore}=a(t)}}_{q_l} = \rho_i L \frac{da}{dt}. \tag{A.2}$$

On the right-hand side of the equation, the first term denotes the heat flux in the ice. The second term is the heat flux in the water and the left-hand side represents the heat induced by water solidification. The boundary conditions are set as the temperature $T \to T_\infty$ as $r_{pore} \to \infty$ (in the grout far from the cavity) and $T = T_i = T_{interf}$ as $r = a$. The spherically solution of the temperature profile is:

$$T_l(r_{pore}, t) = T_\infty + \frac{T_{interf} - T_\infty}{r_{pore}} a(t). \tag{A.3}$$

Note that in this problem, the temperature in the ice is assumed as uniform with the consequence that $q_i = 0$. The gradient of the temperature of the liquid water can be obtained as:

$$\frac{\partial T_l}{\partial r_{pore}}\bigg|_{r_{pore}=a(t)} = -a(t) \frac{T_{interf} - T_\infty}{r_{pore}^2}\bigg|_{r_{pore}=a(t)} = -\frac{T_{interf} - T_\infty}{a(t)}. \tag{A.4}$$

When the temperature at solidification interface T_{interf} (Eq. (A.1)) is replaced in Eq. (A.4) and then injected in the Stefan's heat balance equation (Eq. (A.2)), it yields to the following differential equation that provides the growing

ice radius in a spherically symmetric cavity as:

$$\frac{\partial a}{\partial t}\left[a^2 + aR\frac{\kappa\rho_w^2\rho_i^2L^2}{\lambda_w\mu_0\Delta\rho^2T_0}\right] = \frac{\lambda_l(T_0 - T_{interf})}{\rho_i L}R\frac{\kappa\rho_w^2\rho_i^2L^2}{\lambda_w\mu_0\Delta\rho^2T_0}. \quad (A.5)$$

Appendix B

The strain components given in Eq. (20) are replaced in the equations of the stress components Eqs. (25) and (26) and set into the momentum equilibrium (Eq. (19)), it gives:

$$\frac{\partial^2 u_r}{\partial r^2} + \frac{1}{r}\frac{\partial u_r}{\partial r} - \frac{1}{r^2}u_r = \alpha\frac{\partial\delta T}{\partial r}(1+\nu) - \frac{\partial(p_lS_l + p_iS_i)}{\partial r}\frac{(1+\nu^2)b}{E}. \quad (B.1)$$

Posing to:

$$\tilde{T} = \delta T - (p_lS_l + p_iS_i)\frac{(1-\nu^2)b}{\alpha E(1+\nu)}. \quad (B.2)$$

This equilibrium equation reduces to:

$$\frac{\partial}{\partial r}\left(\frac{1}{r}\frac{\partial}{\partial r}(ru_r)\right) = \alpha\frac{\partial\tilde{T}}{\partial r}(1+\nu). \quad (B.3)$$

After two integrations with respect to r, and by changing the indefinite integral into definite with the boundaries of a circular ring with inner radius r_0 and outer radius r, subjected to axisymmetric temperature change $\delta T = \delta T(r)$, the total displacement can be obtained as:

$$u_r(r) = \frac{(1+\nu)\alpha}{r}\overbrace{\int_{r_0}^{r}\tilde{T}\tau d\tau}^{S} + Ar + \frac{B}{r} \quad (B.4)$$

where A and B are the integral constants. The integration 'S' depends on the boundary conditions in the grout material S_g and in the pipe S_p.

In the pipe:

$$S_p(r) = \int_{r_a}^{r}\delta T_p(r,T)\tau d\tau. \quad (B.5)$$

In the grout:

$$S_g(r) = \int_{r_p}^{r}\tilde{T}\tau d\tau = \int_{r_p}^{r}\left(\delta T_g(r,T) - (p_lS_l + p_iS_i)\frac{(1-\nu_g^2)b}{\alpha_g E_g(1+\nu_g)}\right)\tau d\tau. \quad (B.6)$$

The particular solutions of strain components can be solved as, in the pipe:

$$\varepsilon_{r,p} = \frac{\partial u_{r,p}}{\partial r} = (1+\nu_p)\alpha_p\delta T_p - \frac{(1+\nu_p)\alpha_p S_p(r)}{r^2} + A_p - \frac{B_p}{r^2} \quad (B.7)$$

$$\varepsilon_{\theta,p} = \frac{u_{r,p}}{r} = \frac{(1+\nu_p)\alpha_p S_p(r)}{r^2} + A_p + \frac{B_p}{r^2} \quad (B.8)$$

and in the grout:

$$\varepsilon_{r,g} = \frac{\partial u_{r,g}}{\partial r} = (1+\nu_g)\alpha_g\left[\delta T_g - \frac{(p_lS_l + p_iS_i)(1-\nu_g)b}{\alpha_g E_g}\right] - \frac{(1+\nu_g)\alpha_g S_g(r)}{r^2} + A_g - \frac{B_g}{r^2} \quad (B.9)$$

$$\varepsilon_{\theta,g} = \frac{u_{r,g}}{r} = \frac{(1+\nu_g)\alpha_g S_g(r)}{r^2} + A_g + \frac{B_g}{r^2} \quad (B.10)$$

where the integral constants A_p, B_p, A_g and B_g are deduced in Appendix D.

Finally, the analytical expressions of radial and tangential stresses can be deduced when the strains (Eqs. (B.7)–(B.10)) are introduced in the equations of the stress components (Eqs. (25) and (26)).

Appendix C

The Laplacian temperature change inside the integral can be expressed as:

$$\delta T(r,T) = T_m - T_d\ln(r) \quad (C.1)$$

$$T_m(t) = \Delta T_{in}(t)\frac{\ln(r_{out})}{\ln(r_{out}) - \ln(r_{in})} + \Delta T_{out}(t)\frac{\ln(r_{in})}{\ln(r_{in}) - \ln(r_{out})} \quad (C.2)$$

$$T_d(t) = \frac{\Delta T_{in}(t) - \Delta T_{out}(t)}{\ln(r_{out}) - \ln(r_{in})}. \quad (C.3)$$

The r_{in} and r_{out} represent the radius depending on the boundaries r_a to r_p or r_p to r_b.

By taking the integration of the Laplacian temperature change and setting the components in Eq. (B.6), we obtain in the pipe:

$$S_p(r) = \frac{T_{m,p}(t)(r^2 - r_a^2)}{2} - \frac{T_{d,p}(t)}{2} \times\left(r^2\left(\ln(r) - \frac{1}{2}\right) - r_a^2\left(\ln(r_a^2) - \frac{1}{2}\right)\right) \quad (C.4)$$

and in the grout:

$$S_g(r) = \frac{T_{m,g}(t)(r^2 - r_p^2)}{2} - \frac{T_{d,g}(t)}{2} \times\left(r^2\left(\ln(r) - \frac{1}{2}\right) - r_p^2\left(\ln(r_p^2) - \frac{1}{2}\right)\right) - \frac{(p_lS_l + p_iS_i)(1-\nu_g^2)b}{2\alpha_g E_g(1+\nu_g)}(r^2 - r_p^2). \quad (C.5)$$

Appendix D

(i) From Eq. (27), assuming that the radial stress at the inner radius r_a is zero, the constant B_p can be related to A_p as:

$$\sigma_r(r_a) = 0 \Rightarrow B_p = A_p r_a^2\frac{(1+\nu_p)}{(1-\nu_p)}. \quad (D.1)$$

(ii) Assuming the boundary condition as the stress at the outer-wall radius of the grout r_b is zero, the constant B_g

can be related to A_g as:

$$\sigma_r(r_b) = 0$$
$$\Rightarrow B_g = A_g r_b^2 \frac{(1+\nu_g)}{(1-\nu_g)} - \alpha_g S_g(r_b)(1+\nu_g). \quad \text{(D.2)}$$

(iii) The equality of displacement at the interface between the two materials, $u_{r,g}(r_p) = u_{r,p}(r_p)$ will lead to determine the third integral constant A_g. In the displacement equation given in Eq. (B.4) as $u_{r,g}(r_p)$, when B_g is expressed as a function of A_g (Eq. (D.2)), and similarly in the HDPE pipe as $u_{r,p}(r_p)$, when B_p is expressed as a function of A_p (Eq. (D.1)), it gives:

$$\frac{(1+\nu_g)}{r_p}\left(\frac{A_g r_g^2}{(1-\nu_g)} - \alpha_g\left(S_g(r_b) - \overbrace{S_g(r_p)}^{=0}\right)\right) + A_g r_p = \frac{(1+\nu_p)\alpha_p S_p(r_p)}{r_p} + A_p\left(r_p + \frac{r_a^2}{r_p}\frac{(1+\nu_p)}{(1-\nu_p)}\right) \quad \text{(D.3)}$$

leading to:

$$A_g = \left[C_1 + A_p C_2\right] C_3 \quad \text{(D.4)}$$

with

$$C_1 = \frac{\left(1+\nu_p\right)\alpha_p S_p\left(r_p\right) + \left(1+\nu_g\right)\alpha_g S_g\left(r_b\right)}{r_p} \quad \text{(D.5)}$$

$$C_2 = \left(r_p + \frac{r_a^2}{r_p}\frac{\left(1+\nu_p\right)}{\left(1-\nu_p\right)}\right) \quad \text{(D.6)}$$

$$C_3 = \frac{\left(1-\nu_g\right) r_p}{\left(1+\nu_g\right) r_b^2 + \left(1-\nu_g\right) r_p^2}. \quad \text{(D.7)}$$

(iv) Similarly, to determine the stress equilibrium at the interface $\sigma_{r,g}(r_p) = \sigma_{r,p}(r_p)$ by using Eq. (29), the stress occurred in the pipe determined as the constants B_p, B_g and A_g (Eqs. (D.1), (D.2) and (D.4)) are replaced as a function of the constant A_p:

$$A_p = \frac{\frac{-E_p\alpha_p S_p(r_p) - E_g\alpha_g S_g(r_b)}{r_p^2} - \frac{E_g C_1 C_3}{(1-\nu_g)}\left(1 - \frac{r_b^2}{r_p^2}\right)}{\frac{E_g C_2 C_3}{(1-\nu_g)}\left(1 - \frac{r_b^2}{r_p^2}\right) - \frac{E_p}{(1-\nu_p)}\left(1 - \frac{r_a^2}{r_p^2}\right)}. \quad \text{(D.8)}$$

Finally, once the constants have been determined, the stress components can be calculated in the pipe and in the grout material with respect to the Laplacian temperature differences in the pipe δT_p and in the grout δT_g.

References

[1] Powers TC, Helmuth RA. *Theory of Volume Changes in Hardened Portland Cement Paste During Freezing*. Skokie, Ill: Portland Cement Association; 1953.

[2] Litvan GG. *Phase Transitions of Adsorbates. IV. Mechanism of Frost Action in Hardened Cement Paste*. National Research Council of Canada, Division of Building Research; 1972.

[3] Penttala V. Freezing-induced strains and pressures in wet porous materials and especially in concrete mortars. *Adv Cem Based Mater*. 1998;7(1):8–19.

[4] Penttala V, Al-Neshawy F. Stress and strain state of concrete during freezing and thawing cycles. *Cem Concr Res*. 2002;32(9):1407–1420.

[5] Vlahou I, Worster MG. Ice growth in a spherical cavity of a porous medium. *J Glaciol*. 2010;56(156):271–277.

[6] Style RW, Peppin SSL. The kinetics of ice-lens growth in porous media. *J Fluid Mech*. 2012;692:482–498.

[7] Walder J, Hallet B. A theoretical model of the fracture of rock during freezing. *Geol Soc Am Bull*. 1985;96(3):336–346.

[8] Allan ML, Philippacopoulos AJ. *Properties and performance of cement-based grouts for geothermal heat pump applications. Upton, US-NY, FY 99 Final Report. BNL 67006*. 1999.

[9] Park M, Min S, Lim J, Choi JM, Choi H. Applicability of cement-based grout for ground heat exchanger considering heating–cooling cycles. *Sci China Technol Sci*. 2011;54(7):1661–1667.

[10] Cai H, Liu X. Freeze-thaw durability of concrete: Ice formation process in pores. *Cem Concr Res*. 1998;28(9):1281–1287.

[11] Jacobsen S, Selllevold EJ, Matala S. Frost durability of high strength concrete: Effect of internal cracking on ice formation. *Cem Concr Res*. 1996;26(6):919–931.

[12] Sun W, Zhang YM, Yan HD, Mu R. Damage and damage resistance of high strength concrete under the action of load and freeze-thaw cycles. *Cem Concr Res*. 1999;29(9):1519–1523.

[13] Hanjari KZ, Utgenannt P, Lundgren K. Experimental study of the material and bond properties of frost-damaged concrete. *Cem Concr Res*. 2011;41(3):244–254.

[14] Borinaga-Treviño R, Pascual-Muñoz P, Calzada-Pérez MÁ, Castro-Fresno D. Freeze–thaw durability of cement-based geothermal grouting materials. *Constr Build Mater*. 2014;55:390–397.

[15] Herrmann V. *Ingenieurgeologische Untersuchungen zur Hinterfüllung von Geothermie-Bohrungen mit Erdwärmesonden* [Ph.D. thesis], Karlsruhe, Germany: Fridericiana University of Karlsruhe; 2008 [in German].

[16] Anbergen H, Frank J, Müller L, Sass I. Freeze-thaw cycles on borehole heat exchanger grouts: Impact on the hydraulic properties. *Geotech Test J*. 2014;37(4):20130072.

[17] Erol S, François B. Efficiency of various grouting materials for borehole heat exchangers. *Appl Therm Eng*. 2014;70(1):788–799.

[18] Ineos, Handling book for technical properties of high density polyethylene. INEOS Olefins & Polymers USA. 2009. [Online]. Available: www.ineos-op.com.

[19] Hakagerodur. Hakagerodour-geothermal: Handling book for borehole heat exchangers Technical details of geothermal pipes; Model: Geotherm PE-100., HakaGerodur AG, Benken, CH All. 2010.

[20] Fei Y. Thermal expansion. In: Ahrens TJ, ed. *Mineral Physics and Crystallography—A Handbook of Physical Constants*. AGU Reference Shelf, vol. 2. Washington, USA: American Geophysical Union; 1995:29–44.

[21] Allan M, Philippacopoulos A. Performance characteristics and modelling of cementitious grouts for geothermal heat pumps, 2000: pp. 3355–3360.

[22] Mogensen P. Fluid to duct wall heat transfer in duct system heat storages, In: *Proceedings of the International Conference on Subsurface Heat Storage in Theory and Practice*, 1983: pp. 652–657.

[23] Deerman DJ, Kavanaugh PS. Simulation of vertical U-tube ground—coupled heat pump systems using the cylindrical heat source solution. *ASHRAE Trans*. 1991;97(1):287–295.

[24] Gehlin S. *Thermal Response Test* [Ph.D. thesis], Luleå, Sweden: LuleåUniversity of Technology; 2002.

[25] Lamarche L, Kajl S, Beauchamp B. A review of methods to evaluate borehole thermal resistances in geothermal heat-pump systems. *Geothermics*. 2010;39(2):187–200.

[26] Bejan A, Kraus AD. *Heat Transfer Handbook*. Hoboken, New Jersey: John Wiley & Sons Inc.; 2003.

[27] Hellström G. Thermal performance of borehole heat exchangers. In: *The second Stockton International Geothermal Conference*. 1998.

[28] Voller V, Cross M. Accurate solutions of moving problems using the enthalpy method. *Int J Heat Mass Transfer*. 1981;24:545–556.

[29] Nguyen HT, Wong H, Fabbri A, Georgin JF, Prud'homme E. Analytical study of freezing behavior of a cavity in thermo-poro-elastic medium. *Comput Geotech*. 2015;67:33–45.

[30] Erol S, François B. Thermal stresses in borehole heat exchangers. *Int J Numer Anal Methods Geomech*. 2015;39(13):1450–1470.

[31] Slaughter WS. *The Linearized Theory of Elasticity*. Boston: Birkhaeuser; 2002.

[32] Boley BA, Weiner JH. *Theory of Thermal Stresses*. New York: John Wiley & Sons; 1960.

[33] Biot MA. General theory of three-dimensional consolidation. *J Appl Phys*. 1941;12(2):155–164.

[34] Coussy O, Monteiro PJ. Poroelastic model for concrete exposed to freezing temperatures. *Cem Concr Res*. 2008;38(1):40–48.

[35] Multon S, Sellier A, Perrin B. Numerical analysis of frost effects in porous media. Benefits and limits of the finite element poroelasticity formulation. *Int J Numer Anal Methods Geomech*. 2012;36(4):438–458.

[36] Zuber B, Marchand J. Modeling the deterioration of hydrated cement systems exposed to frost action: Part 1: Description of the mathematical model. *Cem Concr Res*. 2000;30(12):1929–1939.